Journal of Electrostatics 89 (2017) 1–12

Contents lists available at ScienceDirect

Journal of Electrostatics

journal homepage: www.elsevier.com/locate/elstat

Computational study of glow corona discharge in wind: Biased conductor

N.C. Nguyen [a], C. Guerra-Garcia [a, b, *], J. Peraire [a], M. Martinez-Sanchez [a]

[a] Department of Aeronautics and Astronautics, Massachusetts Institute of Technology, Cambridge, MA 02139, United States
[b] Boeing Research & Technology Europe, Madrid, 28042, Spain

ARTICLE INFO

Article history:
Received 9 April 2017
Received in revised form
13 May 2017
Accepted 17 June 2017
Available online 4 July 2017

Keywords:
DC glow corona
Wind
Space charge
Simulation
Kaptzov approximation
Electric field shielding

ABSTRACT

Corona discharges in flowing gas are of technological significance for a wide range of applications, ranging from plasma reactors to lightning protection systems. Numerous experimental studies of corona discharges in wind have confirmed the strong influence of wind on the corona current. Many of these studies report global electrical characteristics of the gaseous discharge but do not present details of the spatial structure of the potential field and charge distribution. Numerical simulation can help clarify the role of wind on the ion redistribution and the electric field shielding. In this work, we propose a methodology to solve numerically for the *drift* region of a DC glow corona using the usual approach of collapsing the ionization region to the electrode surface, but allowing for strong inhomogeneities in the electrical and flow setup. Numerical results for a grounded wire in the presence of an ambient electric field and wind are presented. The model predicts that the effect of the wind is to reduce the extension of the corona over the wire and to shift the center of the ion distribution upstream of the flow. In addition, we find that, even though the near-surface ion distribution is strongly affected by the ion injection law used, the current characteristics and the far field solution remain pretty much unaffected.

1. Introduction

Coronae, electrical discharges localized to the vicinity of an electrode, are ubiquitous in nature and technological applications. They exist in several distinct modes which depend on the time-scale and polarity of the electrical excitation, the electrode configuration, the electrical over-stressing and the relative contribution of build-up versus removal of space charge surrounding the stressed electrode [1,2]. Although the literature on corona discharges is very extensive, some aspects of the corona structure, electric field shielding due to the space charge cloud and its influence on emitted current and mode transition are still a subject of debate [3]. In particular, the detailed effects of a superimposed wind remain unclear.

Corona discharges in flowing gas are of technological significance for plasma reactors, ozone generators, electrostatic precipitators, electrostatic chargers of aerosol particles, or ion drag pumps [4–7]. More recently, ion-driven winds induced by coronae have also been proposed as a propulsion system for small UAVs [8]. Lightning attachment to ground structures, airborne vehicles and windmills [9] is preceded by streamer-corona discharges [10–13]: the implications of wind removal of space charge on electric field shielding [14], and on transition from glow to streamer coronae are of great importance in the prediction of lightning attachment [15,16]. In addition, the influence of wind on coronae from high-voltage DC transmission lines [17] and grounded lightning rods in thunderstorm fields [18] has been a matter of study. Coronae in wind also appear at the sharp extremities of aircraft penetrating thunderstorms [19], the details of these coronae being important since they can generate electromagnetic interference or affect atmospheric electric field measurements performed by instrumented aircraft [20,21].

The windspeed in these problems ranges from tens of cm/s [4] to around 250 m/s [22]. On the other hand, the ion drift speed is ~ 400 m/s (atmospheric air) close to the emitting electrode, but falls rapidly away from the coronating surface. Both drift and windspeed then control the shielding of the applied field due to the presence of a space charge generated by the corona itself and, in turn, the discharge current. If the wind removes the ions effectively, their shielding effect is reduced, necessarily increasing the current [23]

* Corresponding author. Department of Aeronautics and Astronautics, Massachusetts Institute of Technology, Cambridge, MA 02139, United States.
E-mail address: cguerrag@mit.edu (C. Guerra-Garcia).

http://dx.doi.org/10.1016/j.elstat.2017.06.005
0304-3886/

but the influence on the detailed redistribution of the space charge [24] as well as the effect on corona mode transition [25], remain unclear.

In this work, we present a computational study of the influence of wind on the redistribution of the ion cloud generated by a stationary positive glow corona and its impact on the emitted current. The platform under consideration is that of a *biased conductor*, which is representative of laboratory experiments with high voltage electrodes [4–6,8,26], high voltage transmission lines [17] and grounded lightning rods in thunderstorm fields [18]. We present a methodology to solve the coronating surface problem for a highly asymmetric problem (due to geometric and wind effects) using the general approximation of collapsing the ionization region to the surface of the conductor [27]. Future work will extend these studies to include transients, more complex geometries and detailed flow descriptions, as well as incorporate near-electrode physics elements as required to determine the influence of wind in the glow-to-streamer transition.

2. Shielding effect of corona ions and influence of wind

The empirical literature on wind effects on corona discharges is relatively abundant, a classical reference being the study by Chapman [23] in which DC glow coronae were produced from a point electrode in a wind tunnel with wind speeds up to 400 m/s. The experimental results showed a substantial increase of the corona current with wind. In a later paper [28], Chapman reviewed these data as well as others where an external field was applied, and proposed a simplified analytical model that reproduced most of the observed effects. In particular, he concluded that the magnitude of the corona current was affected by the applied voltage, the ion speed (including contributions of the external field and the wind), the presence of nearby electrodes and local conditions at the point.

Since experimental studies primarily deal with the global parameters of the corona (i.e. current-voltage curves) [29], theoretical and computational studies are useful to explain the mechanisms at play. Much of the theoretical work on the electric field modification due to injected space charge is due to the literature on lightning attachment. Semi-analytical and 1D computational models, applied to lightning rods, have suggested that the electric field redistribution due to the space charge of a glow corona (with no wind) hinders the initiation of an upward leader [30–33]. More recently, the authors of [3] extended these studies to two dimensions, and concluded that the shielding effect of the space charge had been overestimated in the lower dimensionality models. According to Becerra's computations [3], the shielding is only strong on the symmetry axis of a vertical lightning rod (no wind is assumed), but it weakens significantly off-axis. For the application of lightning rods, this observation has important consequences in terms of the probability of lightning attachment. By introducing 2D effects, the portion of the rod away from the tip remained unshielded and so lightning attachment could proceed from the radial direction. For our purposes, these studies are relevant since they highlight the importance of an accurate description of the ion cloud to determine its shielding effect, and the implications on the emitted current and corona mode transition. Aside from geometrical considerations, the presence of wind also contributes to this space charge redistribution [24], and is the focus of this work.

3. The Kaptzov approximation for non-symmetric problems

The *positive glow* corona is described by Trinh [2] as *"a thin, luminous layer immediately adjacent to the anode, where intense ionization activity takes place"*. Following these observations, the corona can be described by an *active* region next to the coronating surface, where ionization dominates, and an outer *drift* region, with no ionization, but with net positive (ion) space charge present.

Since the *active* zone is known to be thin, many glow corona calculations collapse the ionization region all the way to the surface of the electrode. For numerical purposes, this means that the surface is at all times at the so-called Peek electric field level, the critical field for corona onset. This modeling approach is generally referred to as the Kaptzov approximation [34], and is supported by experimental evidence [2], as well as comparison to more detailed models [35].

The Kaptzov approximation has been widely used for problems with radial symmetry. In this situation, if a corona forms, it does so uniformly over the coronating conductor and so the Kaptzov approximation requires that the field at the electrode, $E(\boldsymbol{x}) = |\boldsymbol{E}(\boldsymbol{x})\cdot\boldsymbol{n}(\boldsymbol{x})|$, equal the Peek value, E_p. Since the ion density on the electrode needs to be uniform, its value can be determined by gradually increasing it until Peek's condition is met [18].

If there is no radial symmetry, but still the conditions are such that the corona will form over all the electrode surface, the condition $E(\boldsymbol{x}) = E_p$ on the electrode surface still applies, but the ion density on the coronating surface must be allowed to vary circumferentially [27,36], and therefore must be gradually increased in a point-wise manner.

A more complex situation arises when strong asymmetries are present, as is the case of high winds or 3D electrode geometries. In this situation, it can no longer be assumed that the corona covers the full electrode and the region occupied by the corona has to be determined along with the ion density on the electrode surface [37]. The electrode surface $\Gamma_{\text{electrode}}$ is then divided into two disjoint zones: the corona surface Γ_{corona} (where the ion density is not known a priori), and the passive surface Γ_{passive} (where the corona discharge does not occur, and the ion density is zero). The unknown ion density on the corona surface is generally determined by prescribing an injection law [38,39], at the expense of satisfying the Kaptzov condition.

In this work, we generalize Kaptzov's hypothesis to non-symmetric problems due to the presence of strong asymmetries as illustrated in Fig. 1.

On the corona surface, the magnitude of the electric field, $E(\boldsymbol{x})$, is allowed to vary and kept close to the Peek value, thereby residing in a band $[E_p,\ E_p(1+\delta_E)]$. The constant δ_E represents the allowable deviation of the electric field from the Peek value. The ion density $\rho(\boldsymbol{x})$ is a function of the surface field $E(\boldsymbol{x})$, assuming the same dependency as introduced by Ref. [38]:

$$E_p \le E(\boldsymbol{x}) \le E_p(1+\delta_E), \quad \rho(\boldsymbol{x}) = \beta\big(E(\boldsymbol{x}) - E_p\big), \quad \forall \boldsymbol{x} \in \Gamma_{\text{corona}}. \tag{1}$$

To ensure the Kaptzov condition is met, we choose β such that:

$$\max_{\boldsymbol{x}\in\Gamma_{\text{corona}}} E(\boldsymbol{x}) = E_p(1+\delta_E). \tag{2}$$

Note that in previous work [38,39] using this type of injection

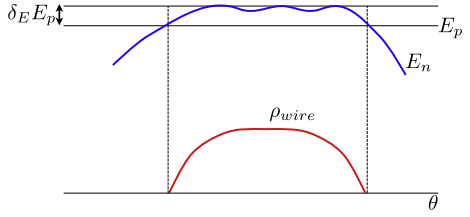

Fig. 1. Generalized Kaptzov approximation to account for strong non-uniformities.

law, the constant β needs to be prescribed by the user of the model.

On the passive surface, the surface field must be lower than the Peek value and the ion density must be zero:

$$E(\boldsymbol{x}) < E_p, \quad \rho(\boldsymbol{x}) = 0, \quad \forall \boldsymbol{x} \in \Gamma_{\text{passive}}. \tag{3}$$

With this modeling approach we can capture the zone occupied by the corona without any prior assumptions on its extension, whilst still satisfying the Kaptzov condition (albeit allowing for uncertainty in its value). Note that even though the uncertainty in the Peek field is introduced as an artifact to impose a generalized Kaptzov condition for non-uniform fields, it can also be justified by physical reasons as will be discussed later.

4. Problem formulation

The 2D problem considered here builds on the models by Mokrov et al. [18], for a lightning rod in the presence of a thunderstorm field, and those of Medlin et al. [27,40], for a high voltage DC transmission line with cross wind.

The electrode configuration under study is pictured in Fig. 2, and consists on a cylindrical grounded wire, of radius $a = 1$ cm, at a height $h = 15$ m above the ground, in the presence of a thunderstorm field, $\boldsymbol{E}_\infty$, and in cross wind. The effect of the ambient electric field $\boldsymbol{E}_\infty$ is to locally enhance the electric field at the wire surface, and a corona discharge is ignited when the onset field is exceeded. For a cylindrical wire in atmospheric pressure air, the onset field is given by the empirical Peek formula [18]:

$$E_p = 3.1\left(1 + 0.0308 a^{-1/2}\right) = 4.05 \text{MV/m}. \tag{4}$$

In the *drift* region, the ions generated by the corona are removed by the combined effect of the external field, and a horizontal wind of magnitude w_∞, which can be modeled assuming potential flow around the cylindrical wire:

$$v_x = w_\infty \frac{a^2 r^2 + r^4 - 2a^2 x^2}{r^4}, \quad v_y = -w_\infty \frac{2a^2 xy}{r^4}, \tag{5}$$

where the coordinates (r, θ), and (x, y) are shown in Fig. 2.

The corona discharge can be described by a drift-diffusion model, neglecting the modification of the air motion due to the ions [41] and possible heating of the air. The *active* corona region is collapsed to the electrode surface, as explained in Section 3, and the *drift* region is described by the system consisting of the continuity equation for the positive ion density and the Poisson equation for the electric field. Only one type of ion is considered and attachment of ions to aerosol particles is not taken into account.

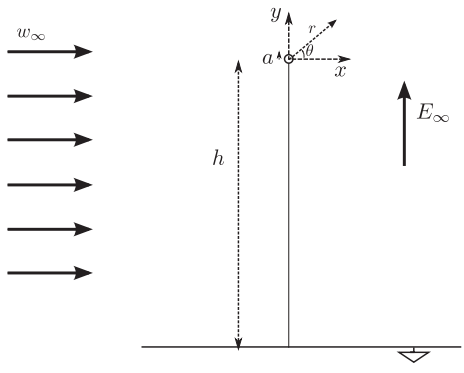

Fig. 2. Geometry and coordinate system for grounded wire in ambient electric field and in the presence of wind.

The problem is solved by separating the effects of the field and potential induced by the corona space charge and the wire charge, $\boldsymbol{E}'$, ϕ' , from that of the thundercloud contribution, $\boldsymbol{E}_\infty$, $-E_\infty(y + h)$. In steady state, the ion continuity equation is given by:

$$\nabla \cdot (\rho(\mu \boldsymbol{E}' + \mu \boldsymbol{E}_\infty + \boldsymbol{v}) - D\nabla\rho) = 0, \tag{6}$$

where μ is the ion mobility, D is the diffusion coefficient, ρ is the ion density and $\boldsymbol{v} = (v_x, v_y)$ is the wind velocity field. The ion density is related to the electric field divergence by Gauss' law:

$$\nabla \cdot \boldsymbol{E}' - \frac{\rho}{\varepsilon_0} = 0, \tag{7}$$

and the field is irrotational and derives from a potential:

$$\boldsymbol{E}' + \nabla\phi' = 0. \tag{8}$$

These equations are solved with the following boundary conditions. We have $\phi' = 0$ and $\nabla\rho \cdot \boldsymbol{n} = 0$ on the ground surface Γ_{ground}. On the wire surface Γ_{wire}, $\phi' = E_\infty h$ and ρ is determined from the conditions given in equations (1)–(3):

$$\phi'(\boldsymbol{x}) = E_\infty h, \quad \rho(\boldsymbol{x}) = \max\{\beta(E(\boldsymbol{x}) - E_p), 0\}, \quad \forall \boldsymbol{x} \in \Gamma_{\text{wire}}. \tag{9}$$

On the far field and outflow boundary, the potential field ϕ' satisfies a Robin condition [42]:

$$\nabla\phi' \cdot \boldsymbol{n} + \frac{\phi'}{r} = 0, \tag{10}$$

while the ion density ρ is set to zero at the inflow boundary. The ion diffusivity is set to $D = 10^{-3}$ m^2/s for numerical reasons but has little influence on the results. The ion mobility is fixed to $\mu = 1.5 \times 10^{-4}$ m^2/V/s.

The current per unit length is calculated by integrating the ion flux at the coronating electrode surface:

$$i = \int_{\Gamma_{\text{corona}}} \rho\mu |\boldsymbol{E}(\boldsymbol{x}) \cdot \boldsymbol{n}| . a d\theta. \tag{11}$$

Here $\boldsymbol{n} = (n_1, n_2)$ is the unit normal vector that points outward from the computational domain.

5. Numerical methods

We use the hybridizable discontinuous Galerkin (HDG) method [43–45] to discretize the partial differential equations (PDEs) in the previous section. First, we write these PDEs into a system of conservation laws as follows

$$\begin{aligned} &\boldsymbol{q} + \nabla \boldsymbol{u} = 0, \\ &\nabla \cdot \boldsymbol{F}(\boldsymbol{u}, \boldsymbol{q}) = \boldsymbol{s}(\boldsymbol{u}), \end{aligned} \tag{12}$$

where $\boldsymbol{u} = (u_1, u_2) \equiv (\phi', \rho)$, $\boldsymbol{q} = (q_1, q_2, q_3, q_4) \equiv -(\partial\phi'/\partial x, \partial\phi'/\partial y, \partial\rho/\partial x, \partial\rho/\partial y)$, $\boldsymbol{s} = (s_1, s_2) \equiv (u_2/\varepsilon_0, 0)$, and

$$\boldsymbol{F} = \begin{pmatrix} F_{11} & F_{12} \\ F_{21} & F_{22} \end{pmatrix} \equiv \begin{pmatrix} q_1 & q_2 \\ \mu u_2 q_1 + u_2 v_1 + D q_3 & \mu u_2 (q_2 + E_\infty) + u_2 v_2 + D q_4 \end{pmatrix}.$$

The PDE system (12) is solved in a computational domain Ω, which is truncated to a distance $R = 100$ m away from the wire as shown in Fig. 3. The boundary conditions for system (12) in the domain Ω are given by

$$\begin{aligned}
u_1 &= 0, && q_3 n_1 + q_4 n_2 = 0, && \text{on } \Gamma_{\text{ground}},\\
u_1 &= E_\infty h, && u_2 = \max\{\beta(|q_1 n_1 + (q_2 + E_\infty) n_2| - E_p), 0\}, && \text{on } \Gamma_{\text{wire}},\\
-q_1 n_1 - q_2 n_2 + \frac{u_1}{R} &= 0, && u_2 = 0, && \text{on } \Gamma_{\text{inflow}},\\
-q_1 n_1 - q_2 n_2 + \frac{u_1}{R} &= 0, && && \text{on } \Gamma_{\text{outflow}}.
\end{aligned} \tag{13}$$

Here Γ_{inflow} (respectively, Γ_{outflow}) is the portion of the domain boundary on which $\boldsymbol{v}_{\text{ion}} \cdot \boldsymbol{n} < 0$ (respectively, $\boldsymbol{v}_{\text{ion}} \cdot \boldsymbol{n} \geq 0$), where $\boldsymbol{v}_{\text{ion}} = \mu \boldsymbol{E}_\infty + \boldsymbol{v}$ is the ion velocity. In particular, Γ_{inflow} is the left boundary, while Γ_{outflow} consists of the right boundary and the top boundary.

To define our numerical approximation, we begin by denoting by $\mathscr{T}_h$ a collection of disjoint regular elements K that partition the domain Ω in a conforming manner, that is, the intersection of the boundaries of any two elements is a face of each of the elements, has zero area or is empty. The set $\partial\mathscr{T}_h := \{\partial K : K \in \mathscr{T}_h\}$ is then a collection of boundaries of the elements. We denote by $\mathscr{E}_h$ the collection of disjoint faces in $\mathscr{T}_h$ and by $\boldsymbol{n}$ the outward normal vector of any face $F \in \mathscr{E}_h$. We next let $\mathscr{P}_m(D)$ denote the space of polynomials of degree at most m on D, and introduce the following approximation spaces (eq. 14):

$$\begin{aligned}
\boldsymbol{U}_{h,p} &:= \left\{ \boldsymbol{w} \in \left[L^2(\mathscr{T}_h)\right]^2 : \boldsymbol{w}|_K \in \left[\mathscr{P}_p(K)\right]^2, \forall K \in \mathscr{T}_h \right\},\\
\boldsymbol{Q}_{h,p} &:= \left\{ \boldsymbol{r} \in \left[L^2(\mathscr{T}_h)\right]^4 : \boldsymbol{r}|_K \in \left[\mathscr{P}_p(K)\right]^4, \forall K \in \mathscr{T}_h \right\},\\
\boldsymbol{M}_{h,p} &:= \left\{ \boldsymbol{\eta} \in \left[L^2(\mathscr{E}_h)\right]^2 : \boldsymbol{\eta}|_F \in \left[\mathscr{P}_p(F)\right]^2, \forall F \in \mathscr{E}_h \right\},
\end{aligned} \tag{14}$$

We then define the inner products for our approximation spaces as

$$\begin{aligned}
(w,v)_{\mathscr{T}_h} &:= \sum_{K \in \mathscr{T}_h} \int_K wv, \quad (\boldsymbol{w},\boldsymbol{v})_{\mathscr{T}_h} := \sum_{j=1}^{n} (w_j, v_j)_{\mathscr{T}_h},\\
\langle w,v \rangle_{\partial\mathscr{T}_h} &:= \sum_{K \in \mathscr{T}_h} \int_{\partial K} wv, \quad \langle \boldsymbol{w},\boldsymbol{v} \rangle_{\partial\mathscr{T}_h} := \sum_{j=1}^{n} \langle w_j, v_j \rangle_{\partial\mathscr{T}_h},
\end{aligned} \tag{15}$$

where n is the number of components of $\boldsymbol{w}$ and $\boldsymbol{v}$. As shown in Fig. 3, the finite element mesh $\mathscr{T}_h$ is comprised of 4197 isoparametric elements and is refined near the wire surface and in the region behind the wire to resolve sharp density gradients in the case of strong crosswinds. We use polynomials of degree $p = 6$ to represent both the numerical solution and the geometry.

To numerically solve system (12) using the HDG method, we seek $(\boldsymbol{q}_h, \boldsymbol{u}_h, \widehat{\boldsymbol{u}}_h) \in \boldsymbol{U}_{h,p} \times \boldsymbol{Q}_{h,p} \times \boldsymbol{M}_{h,p}$ such that

$$\begin{aligned}
(\boldsymbol{q}_h, \boldsymbol{r})_{\mathscr{T}_h} - (\boldsymbol{u}_h, \nabla\cdot\boldsymbol{r})_{\mathscr{T}_h} + \langle \widehat{\boldsymbol{u}}_h, \boldsymbol{r}\cdot\boldsymbol{n} \rangle_{\partial\mathscr{T}_h} &= 0,\\
-(\boldsymbol{F}(\boldsymbol{u}_h, \boldsymbol{q}_h), \nabla\boldsymbol{w})_{\mathscr{T}_h} + \left\langle \widehat{\boldsymbol{f}}_i(\boldsymbol{q}_h, \boldsymbol{u}_h, \widehat{\boldsymbol{u}}_h), \boldsymbol{w} \right\rangle_{\partial\mathscr{T}_h} - (\boldsymbol{s}(\boldsymbol{u}_h), \boldsymbol{w})_{\mathscr{T}_h} &= 0,\\
\left\langle \widehat{\boldsymbol{f}}_i(\boldsymbol{q}_h, \boldsymbol{u}_h, \widehat{\boldsymbol{u}}_h), \boldsymbol{\eta} \right\rangle_{\partial\mathscr{T}_h \backslash \Gamma} + \left\langle \widehat{\boldsymbol{f}}_b(\boldsymbol{q}_h, \boldsymbol{u}_h, \widehat{\boldsymbol{u}}_h), \boldsymbol{\eta} \right\rangle_{\Gamma} &= 0,
\end{aligned} \tag{16}$$

for all $(\boldsymbol{r}, \boldsymbol{w}, \boldsymbol{\eta}) \in \boldsymbol{U}_{h,p} \times \boldsymbol{Q}_{h,p} \times \boldsymbol{M}_{h,p}$, where the interior flux function $\widehat{\boldsymbol{f}}_i(\cdot)$ is defined as

$$\widehat{\boldsymbol{f}}_i(\boldsymbol{q}_h, \boldsymbol{u}_h, \widehat{\boldsymbol{u}}_h) = \boldsymbol{F}(\widehat{\boldsymbol{u}}_h, \boldsymbol{q}_h)\cdot\boldsymbol{n} + \tau(\boldsymbol{u}_h - \widehat{\boldsymbol{u}}_h), \tag{17}$$

and the boundary flux function $\widehat{\boldsymbol{f}}_i(\cdot)$ as

$$\widehat{\boldsymbol{f}}_b = \begin{cases}
\left(\widehat{u}_{h1}, q_{h3} n_1 + q_{h4} n_2 + \tau\left(u_{h2} - \widehat{u}_{h2}\right) \right), & \text{on } \Gamma_{\text{ground}}\\
\left(\widehat{u}_{h1} - E_\infty h, \widehat{u}_{h2} - \max\{\beta(|q_{h1} n_1 + (q_{h2} + E_\infty) n_2| - E_p), 0\} \right), & \text{on } \Gamma_{\text{wire}}\\
\left(-q_{h1} n_1 - q_{h2} n_2 + \frac{\widehat{u}_{h1}}{R} + \tau\left(u_{h1} - \widehat{u}_{h1}\right), \widehat{u}_{h2} \right), & \text{on } \Gamma_{\text{inflow}}\\
\left(-q_{h1} n_1 - q_{h2} n_2 + \frac{\widehat{u}_{h1}}{R} + \tau\left(u_{h1} - \widehat{u}_{h1}\right), u_{h2} - \widehat{u}_{h2} \right), & \text{on } \Gamma_{\text{outflow}}.
\end{cases} \tag{18}$$

Note that the definition of the boundary flux function $\widehat{\boldsymbol{f}}_b(\cdot)$ varies on the boundary domain Γ since the boundary conditions (13) are different on each portion of the domain boundary.

The structure of the HDG method makes itself amenable to an efficient implementation. Indeed, note that the first two equations in (16) can be thought as giving $\boldsymbol{q}_h$ and $\boldsymbol{u}_h$ in terms of $\widehat{\boldsymbol{u}}_h$. The last equation in (16) is then the equation that determines the actual values of the unknown $\widehat{\boldsymbol{u}}_h$; it actually enforces the single-valuedness of the tangential component of the numerical flux $\widehat{\boldsymbol{f}}_i$ and imposes the boundary conditions. In this manner, the only globally-coupled degrees of freedom are those of $\widehat{\boldsymbol{u}}_h$ after linearizing the HDG formulation (16) by the Newton method and locally eliminating the degrees of freedom of $\boldsymbol{q}_h$ and $\boldsymbol{u}_h$ by static condensation. We refer to [43–45] for a detailed discussion about the implementation of the HDG method.

It remains to describe an algorithm for finding β to satisfy condition (2). If the constant β is initialized to an appropriate value,

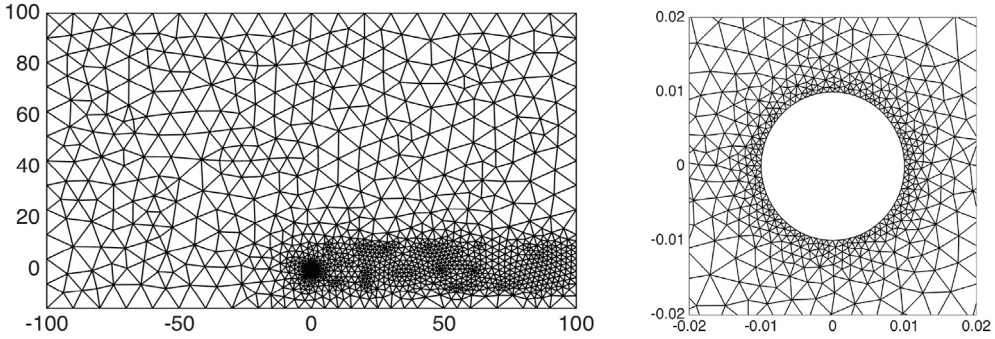

Fig. 3. Finite element mesh and a close-up view of the mesh near the wire. x and y axes are in [m].

then we can solve problem (12) using the HDG method to obtain the electric field $E(\boldsymbol{x},\beta)$ on the wire. We set $E_{\max}(\beta) = \max_{\boldsymbol{x}\in\Gamma_{\text{wire}}} E(\boldsymbol{x},\beta)$. It is important to note that $E_{\max}(\beta)$ is a monotonically decreasing function of β. This allows us to solve the equation $E_{\max}(\beta) = (1+\delta_E)E_p$ for β by using the bisection algorithm. First, we find β_l such that $E_{\max}(\beta_l) > (1+\delta_E)E_p$ and β_u such that $E_{\max}(\beta_u) < (1+\delta_E)E_p$. Hence, β must reside in the interval $[\beta_l,\beta_u]$. Next, we shrink the interval $[\beta_l,\beta_u]$ as follows: if $E_{\max}((\beta_l+\beta_u)/2) > (1+\delta_E)E_p$ then we set $\beta_l = (\beta_l+\beta_u)/2$ and $\beta_u = \beta_u$; but if $E_{\max}((\beta_l+\beta_u)/2) < (1+\delta_E)E_p$ then we set $\beta_l = \beta_l$ and $\beta_u = (\beta_l+\beta_u)/2$. We repeat this step until $E_{\max}((\beta_l+\beta_u)/2) = (1+\delta_E)E_p$ and return $\beta = (\beta_l+\beta_u)/2$.

6. Numerical results

The minimum ambient field for corona inception, E_i, is given by the condition that the surface field be amplified to the Peek value. For the setup in Fig. 2, and $a << h$, this field is:

$$E_i \approx E_p \frac{a}{h}\ln(2h/a) = 21.6kV/m. \tag{19}$$

The results presented in this section investigate the influence of

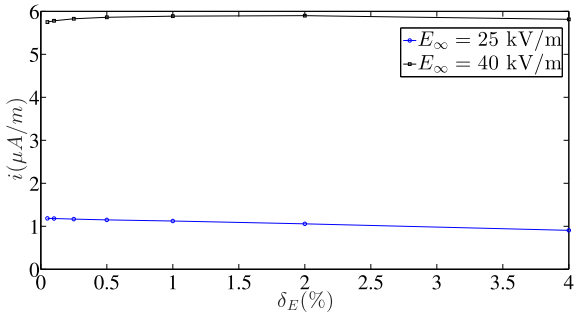

Fig. 5. Corona current per unit length as a function of $\delta_E(\%)$. $w_\infty = 20$ m/s.

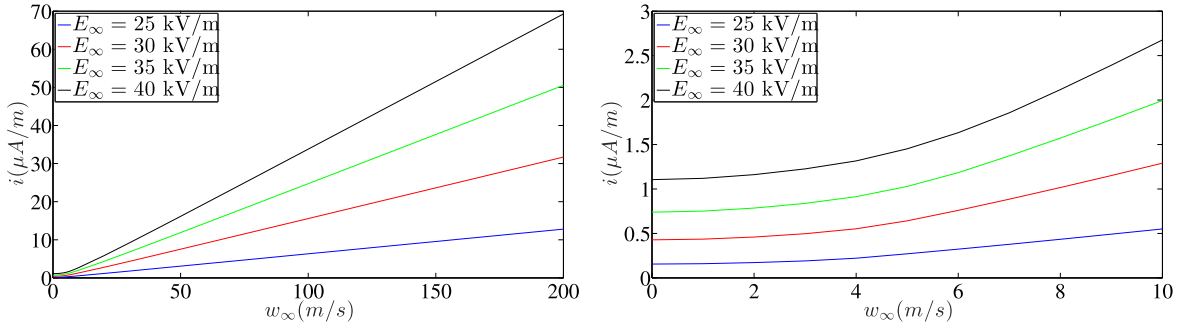

(a) Strong wind.

(b) Moderate wind.

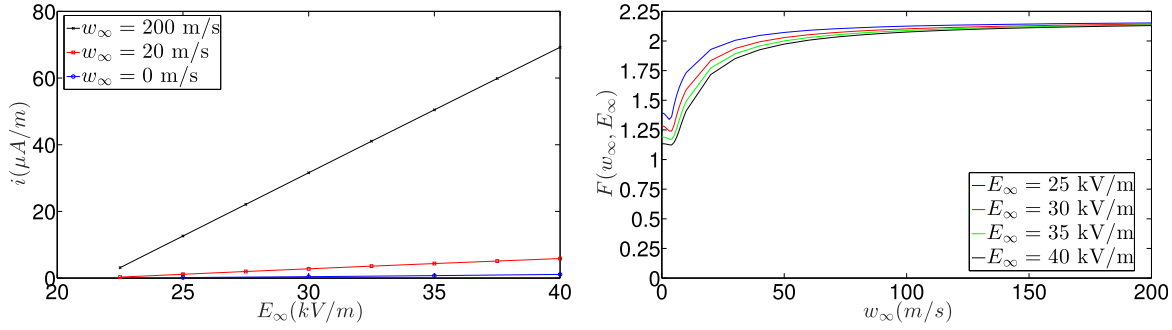

(c) Dependency with field.

(d) $F(w_\infty, E_\infty)$.

Fig. 4. Corona current per unit length as a function of w_∞ for different values of E_∞. The error band in the Peek field was chosen as $\delta_E = 0.25\%$.

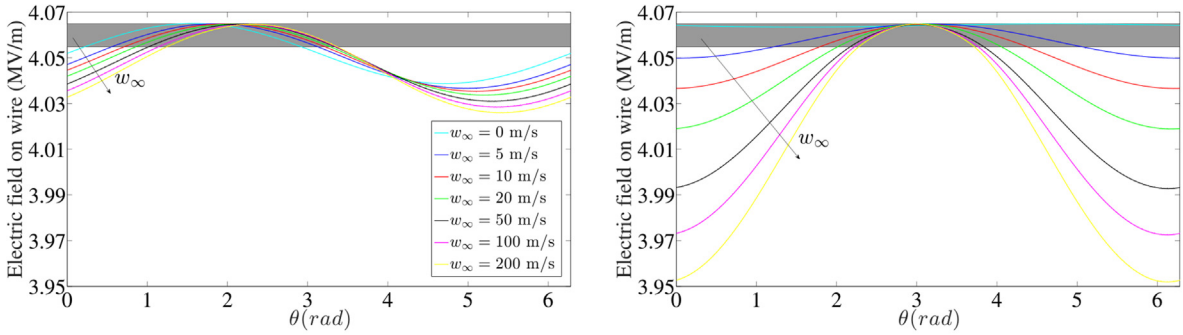

(a) $E_\infty = 25$ kV/m. (b) $E_\infty = 40$ kV/m.

Fig. 6. Electric field intensity on the wire for different values of (w_∞, E_∞). The uncertainty in the Peek value is $\delta_E = 0.25\%$. The grey band indicates the region occupied by the corona.

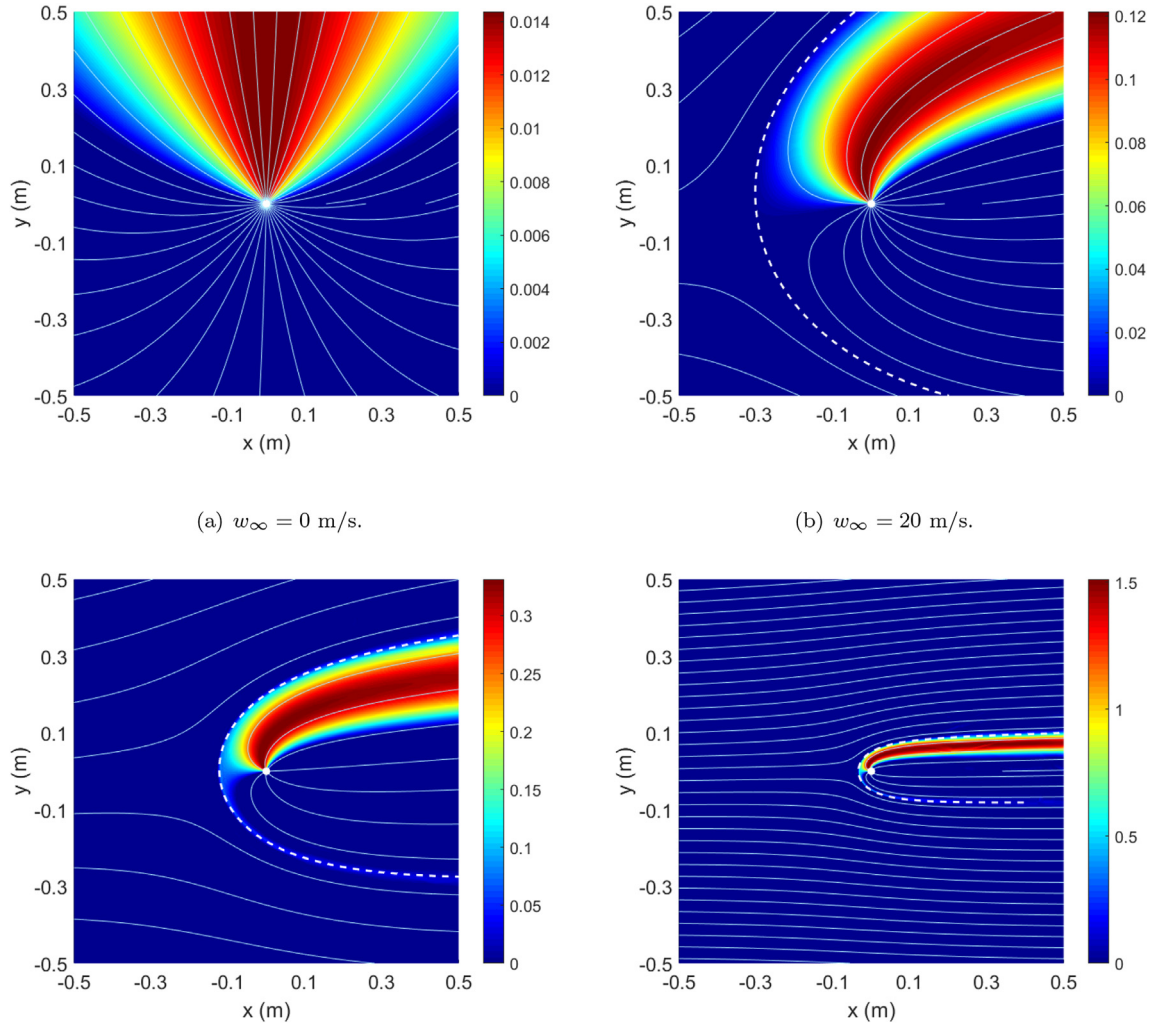

(a) $w_\infty = 0$ m/s. (b) $w_\infty = 20$ m/s.

(c) $w_\infty = 50$ m/s. (d) $w_\infty = 200$ m/s.

Fig. 7. Influence of wind on ion density $[\mu C/m^3]$ near wire. $E_\infty = 25$ kV/m, $\delta_E = 0.25\%$.

$E_\infty > E_i$, w_∞, and the arbitrary choice of δ_E, on the emitted current and the corona structure.

6.1. Corona current characteristics in wind and ambient field

The influence of wind and field on the corona current has been evaluated for fixed uncertainty band in the Peek field, as shown in Fig. 4. Many semi-empirical formulas have been reported in the literature for the dependency of current with wind and field, very often of the type [23,29]:

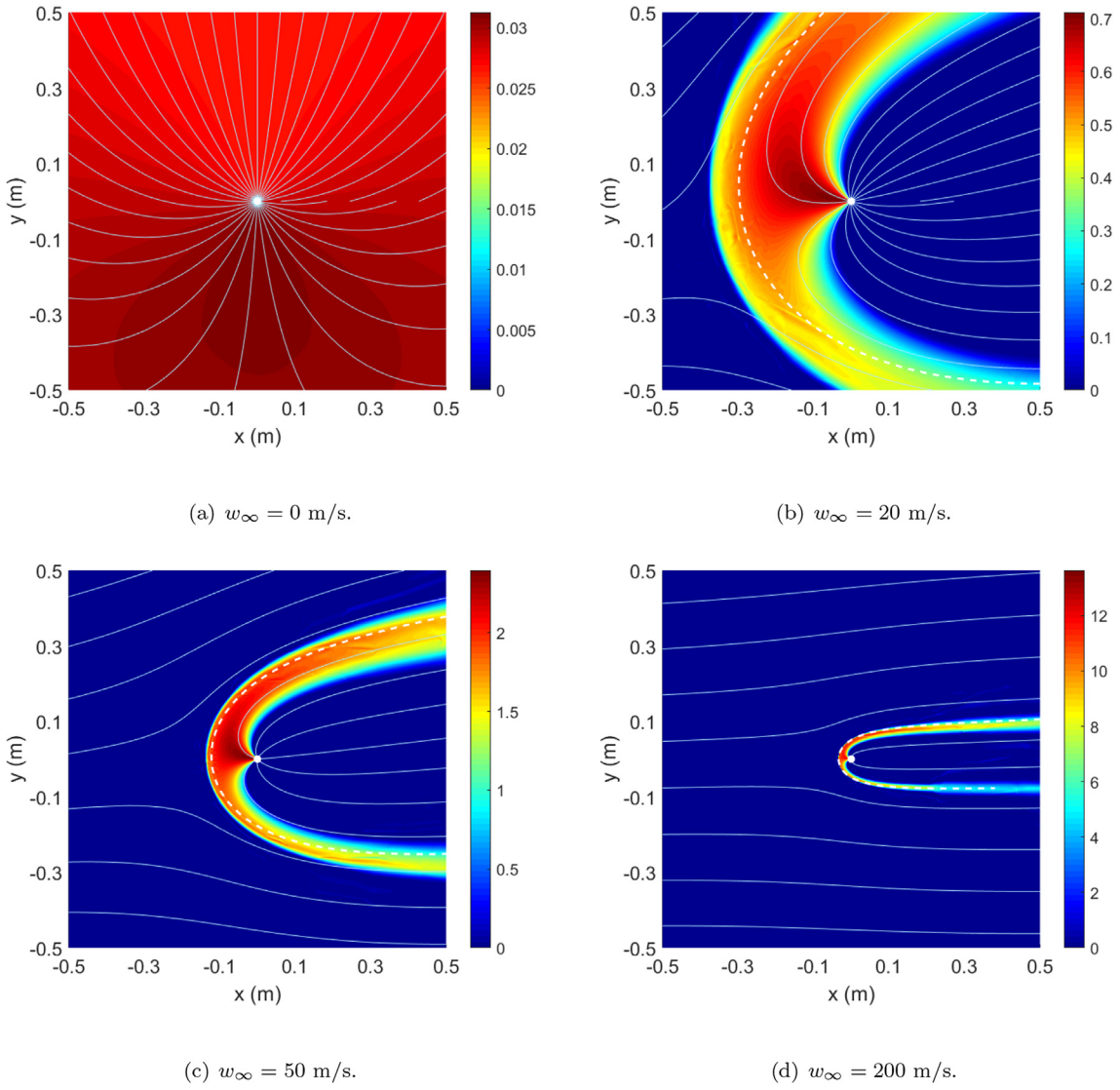

(a) $w_\infty = 0$ m/s. (b) $w_\infty = 20$ m/s.

(c) $w_\infty = 50$ m/s. (d) $w_\infty = 200$ m/s.

Fig. 8. Influence of wind on ion density [$\mu C/m^3$] near wire. $E_\infty = 40$ kV/m, $\delta_E = 0.25\%$.

$$i = F v_{\text{ion}}^{\infty} \varepsilon_0 (E_\infty - E_i), \tag{20}$$

where i is the current per unit length; $v_{\text{ion}}^{\infty} = \sqrt{(\mu E_\infty)^2 + w_\infty^2}$ is the ion velocity far from the wire; and F a non-dimensional constant, of order one, which accounts for the geometrical configuration of the electrical setup. For laboratory setups [23], cites differences of a factor of 2–5 in F for point-to-plate or point between parallel plates configurations.

The numerical results shown in Fig. 4 have been fitted to equation (20) to find the parameter F. Fig. 4(d) shows that F depends on wind and field, $F = F(w_\infty, E_\infty)$, and is of order one but not a constant for intermediate wind speeds. For high wind and the considered geometry $F \sim 2.1$. These dependencies are not surprising since the electrical configuration is modified by the presence of the space charge which depends on field and wind. Note that experiments by Ref. [23] also show differences in the multiplying constant (here F) when the wind is dominant, as compared to no wind.

For strong wind, i.e. $w_\infty >> \mu E_\infty$, the current has a linear dependency with both wind and field, and the wind dominates the ion evacuation process. For low wind velocity, i.e. $w_\infty << \mu E_\infty$, the corona current is almost independent of the wind and quadratic with the field, and the ion evacuation is dominated by the electric drift.

Note that by ignoring the near-wall physics (*the active region*), a possible effect of wind on the threshold external field for corona initiation, E_i, cannot be captured.

As a sanity check, the influence of the uncertainty in the Peek value, δ_E, on the current characteristics has been evaluated, see Fig. 5. For a variation in the uncertainty of the Peek field between 0.05%-4%, the corona current per unit length is practically unaffected by choice of this value.

6.2. Ion cloud in wind and ambient field

More interestingly, the simulations show the effect of wind on the ion distribution near the wire, Figs. 7 and 8. The electric field on the electrode surface, is shown in Fig. 6.

The first observation is that, regardless of the extension of the *corona surface*, the electric field on the wire remains close to the Peek value. For the parameter range considered, the azimuthal variation in the electric field is below 3%, and the maximum deviation is encountered for maximum injected charge (maximum

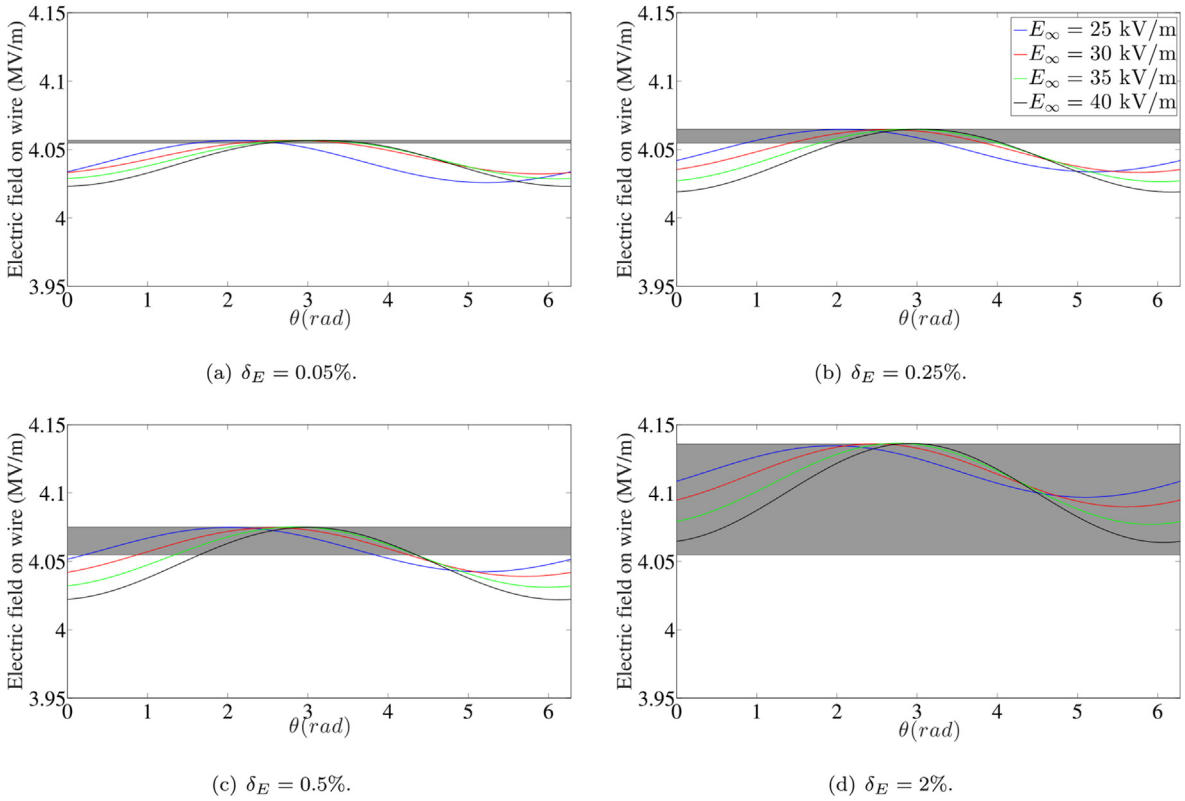

(a) $\delta_E = 0.05\%$. (b) $\delta_E = 0.25\%$.

(c) $\delta_E = 0.5\%$. (d) $\delta_E = 2\%$.

Fig. 9. Electric field intensity distribution on the wire for different (E_∞, δ_E). $w_\infty = 20$ m/s. The grey band indicates the region occupied by the corona.

wind and field), Fig. 6(b). For the considered geometry, this approximately uniform field on the wire surface, even for an ion density that is not, has also been reported by Ref. [27]. The extent of the corona surface is in fact dependent on both field and wind.

For an ambient field that is close to the corona inception threshold e.g. $E_\infty = 25$ kV/m, Figs. 6(a) and (7), a small amount of charge flux injection is sufficient to satisfy the Peek condition. For the no-wind scenario, as soon as that charge is injected from the region of maximum field on the wire ($\theta = \pi/2$), it shields all the wire below the Peek threshold, and so a partial corona is sufficient to satisfy the generalized Kaptzov condition of section 3. The situation is qualitatively similar in the presence of wind, thus the extension of the corona surface is similar to the no-wind case although the center of the ion distribution shifts upstream of the flow.

The ion density near the wire for the case $E_\infty = 25$ kV/m is plotted in Fig. 7. Superimposed to the numerical results (in light blue) are the analytical ion streamlines when substituting the contribution of the space charge and the wire charge by that of a charged wire that satisfies Kaptzov on its surface:

$$\Psi = \mu E_p a\theta + w_\infty\left(r - \frac{a^2}{r}\right)\sin\theta - \mu E_\infty\left(r - \frac{a^2}{r}\right)\cos\theta. \tag{21}$$

The streamfunction that goes through the stagnation point, Ψ_s, is:

$$\Psi_s = \mu E_p a\theta_s, \quad \theta_s = \tan^{-1}\left(\frac{\mu E_\infty}{w_\infty}\right), \tag{22}$$

and is indicated by the white dashed line. This separatrix separates the region occupied by the ion cloud from the no-charge region, and closely follows the numerical results that account for the actual space and wire charge.

For a stronger ambient field, that amplifies the electric field on the wire significantly beyond the Peek threshold, the charge flux injected needs to be larger (e.g. for $E_\infty = 40$ kV/m, the field on the wire ignoring the space charge is $|\boldsymbol{E}\cdot\boldsymbol{n}| \approx 1.85E_p$). Thus, for the no-wind case, the full wire surface is occupied by the corona, Figs. 6(b) and 8, to ensure Kaptzov is met everywhere. The situation differs in the presence of wind, the corona region becomes smaller as the wind becomes stronger, and the localized charge injection is sufficient to shield the rest of the wire surface. The center of the ion distribution is at $\theta \approx \pi$, and the appearance of the ion distribution near the wire can again be explained by the ideal streamlines when substituting the effect of the ion cloud and the wire charge by a charged wire that satisfies Kaptzov, Fig. 8. In this case the discrepancy is larger since the distortion of the laplacian electric field will be stronger as a consequence of the higher ion densities encountered.

The influence of the wind far from the wire is the development of a positive ion plume in the direction $\tan\theta \approx \mu E_\infty / w_\infty$ that acts to reduce the electric field between plume and ground plane, Fig. 11, due to an induced field in the downwards direction.

6.3. *Distributed versus spot mode coronae: influence of uncertainty band in peek's threshold*

The uncertainty band in the Peek threshold was an artifact introduced in the solution methodology proposed in section 3. It was shown that the choice of δ_E had little effect on the global properties of the corona and, in particular, on the current characteristics, Fig. 5. However, the uncertainty in the Peek value has a strong influence on the ion distribution close to the wire as is shown in Figs. 9 and 10.

Fig. 9 shows the impact of the choice of δ_E on the electric field on

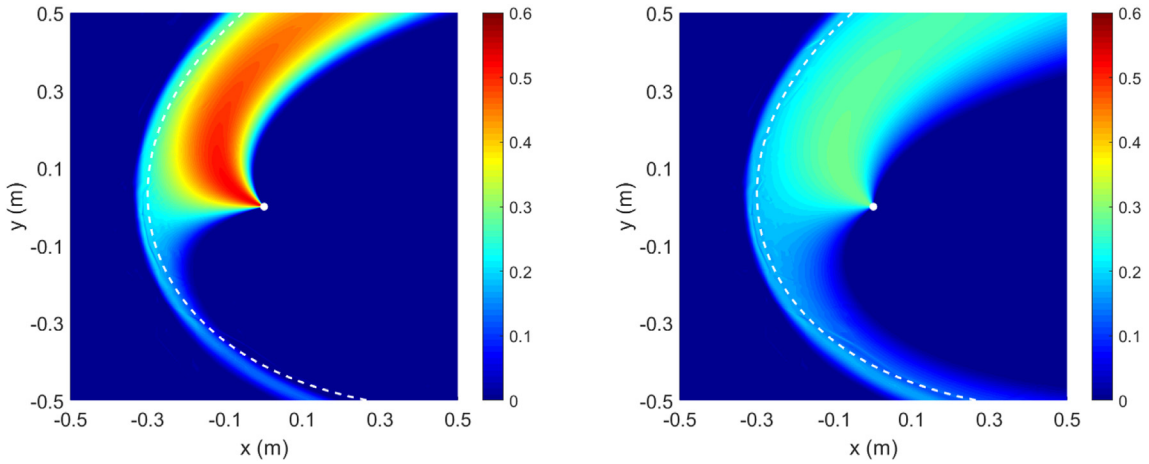

(a) $\delta_E = 0.05\%$. (b) $\delta_E = 0.25\%$.

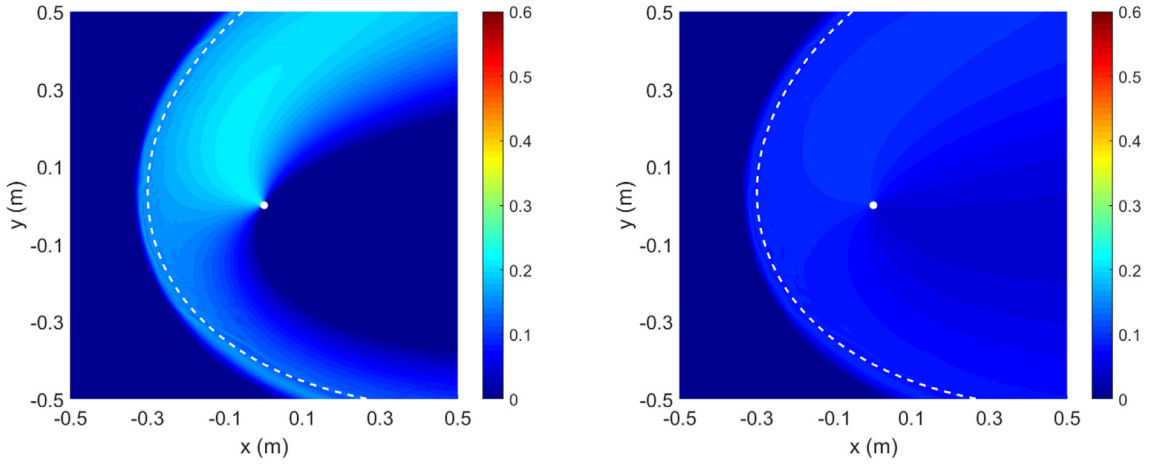

(c) $\delta_E = 0.5\%$. (d) $\delta_E = 2\%$.

Fig. 10. Ion distribution $[\mu C/m^3]$ near wire for different δ_E. $w_\infty = 20$ m/s, $E_\infty = 30$ kV/m.

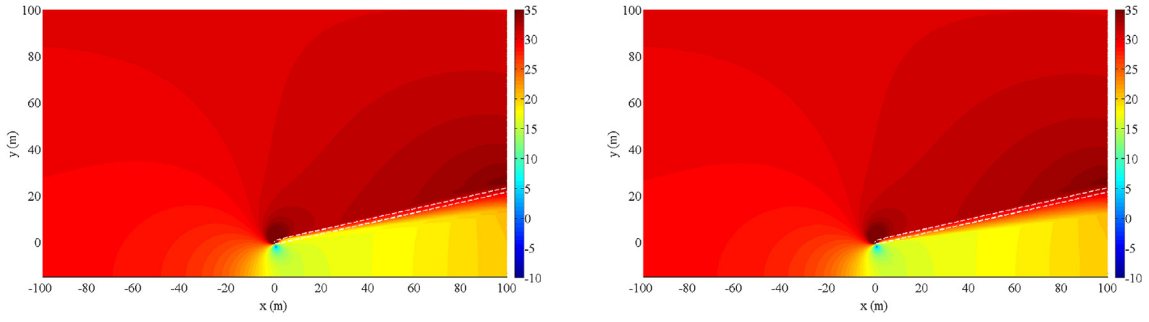

(a) $\delta_E = 0.05\%$. (b) $\delta_E = 2\%$.

Fig. 11. Effect of δ_E on the electric field amplitude $[kV/m]$. $w_\infty = 20$ m/s, $E_\infty = 30$ kV/m.

the wire, for a wind speed of $w_\infty = 20$ m/s and several ambient field values. In all cases, the observed azimuthal variation of the electric field on the wire is below 2%. Thus, for δ_E below this value, a *spot* or *localized* corona is observed, whereas for $\delta_E \sim 2\%$ the corona is a *distributed* corona that occupies all the wire surface. The extension of the *corona surface* increases with δ_E.

Fig. 10 shows, for different δ_E, the ion distribution near the wire. The ion streamlines, as well as the center of the ion distribution, are pretty much unaffected by the choice of δ_E, however, the extent of the corona surface is dependent on δ_E. For lower δ_E, the corona

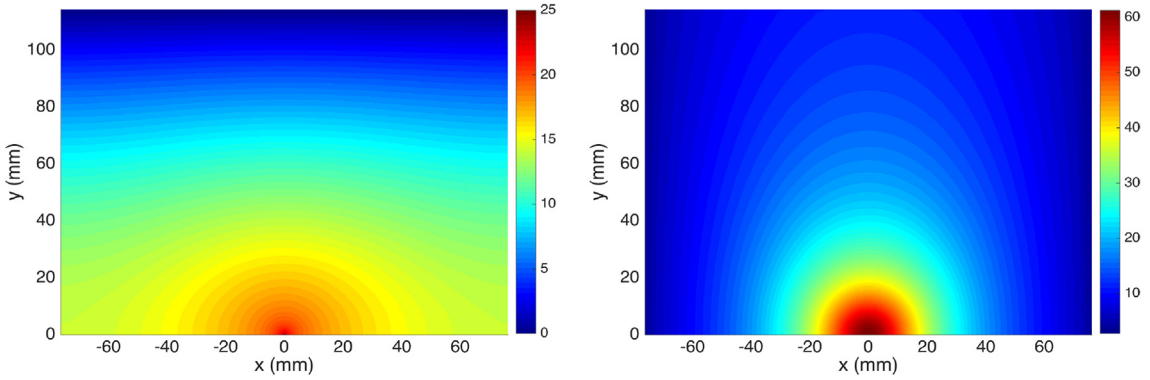

Fig. 12. Electric potential (kV) (left) and ion density (μC/m^3) (right) for the second test case.

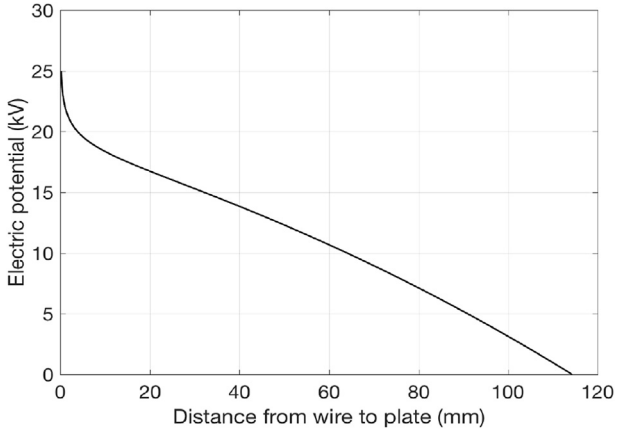

Fig. 13. Electric potential along the line from the discharge electrode to the collecting electrode for our numerical simulation: compare to Fig. 8 in Ref. [7] which shows numerical simulations by Ref. [7] and experimental measurements by Ref. [46].

region is more localized, but the ion densities are higher. For higher δ_E, the corona occupies a larger region, but the ion densities are smaller. So, even though the ion distribution differs on the wire region, the charge flux being injected remains pretty much the same.

From a practical perspective, the little dependency of the injection law on the global response, i.e. the current characteristics (Fig. 5) and the far field solution (Fig. 11), is an important result since there is no consensus in the literature on this aspect [27,36–39]. If the near electrode solution is not required, the choice of injection law does not significantly affect the results.

From a physics perspective, the threshold Peek field will also vary azimuthally on the wire, since local roughness of the surface, as well as local heating, can affect its value. Also, a variation of the Peek value is expected due to the non-symmetric distribution of the space charge and field (note that equation (4) is derived assuming a 1D cylindrical Laplacian field). Thus, accounting for a finite variation in E_p also helps visualize the natural variations in the corona threshold. It is interesting to note that the expected current and the solution far from the wire are similar whether the corona is a *spot mode* or a *distributed mode* corona.

7. Conclusions

We have presented a methodology to solve the problem of a DC glow corona in the presence of strong asymmetries using the usual approach of collapsing the *active region* to the electrode surface. In this work, the asymmetry was introduced by a strong cross wind, but a similar approach can be used to deal with complex electrode configurations. The generalized Kaptzov model proposed allows to solve for the corona surface over the wire, while still satisfying the Peek field condition on the wire surface within an uncertain Peek threshold. Future investigations will need to determine how to select the band in the Peek field to define the real ion distribution on the surface.

Numerical results of a corona in wind are presented for the case of a grounded wire in ambient field and potential flow wind. The current-field and current-wind characteristics computed show the expected dependencies. For $w_\infty >> \mu E_\infty$, the wind dominates the ion evacuation process; whereas for $w_\infty << \mu E_\infty$, the electrical drift is dominant.

Aside from significantly increasing the corona current, the effect of the wind is to localize the corona (reduce the extent of the wire surface occupied by the discharge) and to shift the center of the ion distribution on the wire upstream of the flow. A simplified model that substitutes the space and wire charge by a charged wire that satisfies Kaptzov was used to explain the localization of the ion cloud inside a separatrix surface.

An observation from this numerical study was the practical independence of the emitted current, and of the solution far from the wire, with the specific injection law used. This indicates that for the geometry considered (isolated wire in field and wind) the distant space charge drives the magnitude of the current. This has the practical implication that the predicted current will not be greatly influenced by the injection law used, which is important since there is no consensus in the literature. In terms of physical implications, local effects of roughness or heating on the wire surface will act to localize the corona to a specific region on the wire (*spot* versus *distributed* modes) but the expected effect on the global properties is small.

This manuscript has presented numerical validation of our methods, see Appendix A. Future work will extend these studies to account for transients, more complex geometries, detailed flow effects, as well as incorporate the necessary physics to allow prediction of the glow-to-streamer corona transition.

Acknowledgments

This work was funded by The Boeing Company through the Strategic Universities for Boeing Research and Technology Program. The authors would like to thank Benjamin Westin and Terry Vogler (Boeing) for their continued support. N C Nguyen and J Peraire acknowledge partial support from the Air Force Office of Scientific Research (AFOSR) through Grant No. FA9550-16-1-0214.

Appendix A. Numerical verification and validation

The numerical models and methods presented in this manuscript have been verified and validated, to the extent possible, through comparison with available analytical, numerical and experimental results. In particular, good correspondence is found with: (1) the analytical solution to a cylindrical electrostatic precipitator reported in Ref. [7] (section A.1); (2) numerical results by Ref. [7] and experimental measurements by Ref. [46] for a wire-plate electrostatic precipitator (section A.2); (3) numerical results by Ref. [27] and experimental results by Ref. [47] for a DC high voltage line to plane geometry (no wind); (4) numerical results by Refs. [27,36] for a DC high voltage line to plane geometry in the presence of wind. For brevity, only cases (1) and (2) are summarized in what follows.

A.1. Analytical solution

This problem taken from Ref. [7] serves to verify the HDG method since it has an exact solution. A cylindrical electrostatic precipitator consists of a circular wire as the discharge electrode and an earthed coaxial cylinder (pipe) as the collecting electrode. The geometry of the electrostatic precipitator is defined by the radii of the wire and pipe, a and b, respectively. For zero ion diffusion, the problem has the following analytical solution

$$\phi(r) = -\sqrt{d\cdot b^2+c^2}+\sqrt{d\cdot r^2+c^2}+c\ln\left(\frac{r}{b}\right)+c\ln\left(\frac{c+\sqrt{d\cdot b^2+c^2}}{c+\sqrt{d\cdot r^2+c^2}}\right),$$
$$\rho(r) = \frac{\varepsilon_0\cdot d}{\sqrt{d(r^2-a^2)+a^2\cdot E_p^2}}, \tag{23}$$

where $r=\sqrt{x^2+y^2}$, $d=\frac{J_0}{2\pi\varepsilon_0\mu}$ and $c=a\sqrt{E_p^2-d}$. J_0 is the current per unit length. We choose $J_0=2\pi$, $a=1$, $b=10$, $\mu=1$, $\varepsilon_0=1$, and $E_p=\sqrt{2}$, so that we have $c=d=1$. We use a mesh of 392 triangular elements and polynomials of degree $p=4$ to represent the numerical solution. The absolute error in both ϕ and ρ is less than 10^{-5} in all the solution domain, proving the accuracy of the method.

A.2. Corona discharge of wires between two collecting plates

The row of wires (discharge electrodes) between two plates (collecting electrodes) is a typical configuration of a wire-plate electrostatic precipitator. The geometry parameters are defined by $a=0.152$ mm, $b=114.3$ mm, $c=52.4$ mm, where $2a$ is the diameter of the wires, $2b$ is the distance between the two plates, and $2c$ is the distance between two consecutive wires. The ion diffusivity is zero, while the ion mobility $\mu=2\times10^{-4}$ m^2/V/s. The electric potential on the wire surface is set to 25 kV. The ion density on the wire surface is calculated from the condition $|\boldsymbol{E}\cdot\boldsymbol{n}|=E_p$ using $E_p=10.092$ MV/m. On the collecting plate, we have zero electric potential and zero ion density flux. We refer to [7,46] for a more detailed description of the problem.

We solve the problem on a computational domain that includes a single wire by exploiting the symmetry of the problem. We discretize the computational domain into 4344 triangular elements and polynomials of degree $p=2$ are used to represent the numerical solution. Fig. 12 shows contours of the electric potential ϕ and ion density ρ. Fig. 13 displays the electric potential along the line from the discharge electrode (wire) to the collecting electrode (plate), to be compared to Fig. 8 in Ref. [7] (which shows numerical simulations by Ref. [7] and experimental measurements by Ref. [46]). Our simulation results are in good agreement with numerical results of [7], and experimental results of [46].

References

[1] N.G. Trinh, J.B. Jordan, Modes of corona discharges in air, IEEE Trans. Power apparatus Syst. PAS 87 (5) (1968) 1207–1215.
[2] N.G. Trinh, Discharge in air. Part I: physical mechanisms, IEEE Electr. Insul. Mag. 11 (2) (1995) 23–29.
[3] M. Becerra, Glow Corona Discharges and Their Effect on Lightning Attachment: Revisited, International Conference on Lightning Protection (ICLP), Vienna, Austria, 2012.
[4] A. Jaworek, A. Krupa, Corona discharge from a multipoint electrode in flowing air, J. Electrost. 38 (1996) 187–197.
[5] T. Yamamoto, P.A. Lawless, L.E. Sparks, Narrow-gap point-to-plane corona with high velocity flows, IEEE Trans. Industry Appl. 24 (5) (1988) 934–939.
[6] O.M. Stuetzer, Ion drag pumps, J. Appl. Phys. 31 (1) (1960) 136–146.
[7] N. Neimarlija, I. Demirdzic, S. Muzaferija, Finite volume method for calculation of electrostatic fields in electrostatic precipitators, J. Electrost. 67 (2009) 37–47.
[8] C.K. Gilmore, S.R.H. Barrett, Electrohydrodynamic thrust density using positive corona-induced ionic winds for in-atmosphere propulsion, Proc. R. Soc. Lond. A 471 (2015) 20140912.
[9] J. Montanya, O. van der Velde, E.R. Williams, Lightning discharges produced by wind turbines, J. Geophys. Res. Atmos. 119 (2014) 1455–1462.
[10] I. Gallimberti, The mechanism of the long spark formation, J. de Physique Colloques 40 (C7) (1979). C7–193–C7–250.
[11] I. Gallimberti, G. Bacchiega, A. Bondiou-Clergerie, P. Lalande, Fundamental processes in long air gap discharges, C. R. Phys. 3 (2002) 1335–1359.
[12] A. Larsson, The interaction between a lightning flash and an aircraft in flight, C. R. Phys. 3 (2002) 1423–1444.
[13] P. Lalande, A. Bondiou-Clergerie, G. Bacchiega, I. Gallimberti, Observations and modeling of lightning leaders, C. R. Phys. 3 (2002) 1375–1392.
[14] S. Vogel, J. Lopez, J. Holboll, S.F. Madsen, A.C. Garolera, K. Bertelsen, Numerical simulation of the effect of wind removing the corona space charge over grounded structures under thunderstorm conditions, International Conference on Lightning and Static Electricity (ICOLSE), Toulouse, France, 2015.
[15] L. Liu, M. Becerra, On the transition from stable positive glow corona to streamers, J. Phys. D. Appl. Phys. 49 (22) (2016) 225202.
[16] J.R. Dwyer, M.A. Uman, The physics of lightning, Phys. Rep. 534 (2014) 147–241.
[17] P.S. Maruvada, Influence of wind on the electric field and ion current environment of HVDC transmission lines, IEEE Trans. Power Deliv. 29 (6) (2014) 2561–2569.
[18] M.S. Mokrov, Y.P. Raizer, E.M. Bazelyan, Development of a positive corona from a long grounded wire in a growing thunderstorm field, J. Phys. D. Appl. Phys. 46 (2013) 455202.
[19] J.J. Jones, Electric charge acquired by airplanes penetrating thunderstorms, J. Geophys. Res. 95 (D10) (1990) 16589–16600.
[20] X. Da, H. Shen, L. Hong, Magnitude of corona current caused by aircraft net charge, J. Aircraft 46 (3) (2009) 1005–1008.
[21] X. Da, H. Shen, L. Hong, R. Zhang, Unmanned air vehicle wing-tip corona nonlinear effect on atmospheric electric field measurements, J. Aircraft 46 (5) (2009) 1714–1720.
[22] V. Mazur, A physical model of lightning initiation on aircraft in thunderstorms, J. Geophys. Res. 94 (D3) (1989) 3326–3340.
[23] S. Chapman, Corona point current in wind, J. Geophys. Res. 75 (12) (1970) 2165–2169.
[24] Y. Zou, J. He, H. He, Effect of wind on the distribution of the corona discharge ionized field generated from grounded wire during thunderstorms, International Conference on Lightning Protection (ICLP), Shanghai, China, 2014, pp. 879–884.
[25] M. Becerra, V. Cooray, S. Soula, S. Chauzy, Effect of the space charge layer created by corona at ground level on the inception of upward lightning leaders from tall towers, J. Geophys. Res. 112 (2007) D12205 (11pp).
[26] Les Renardières, Research on long air gap discharges at Les Renardières, ELECTRA 23 (1972) 53–157.
[27] A.J. Medlin, R. Morrow, C.A.J. Fletcher, Calculation of monopolar corona at a high voltage DC transmission line with crosswinds, J. Electrost. 43 (1998) 61–77.
[28] S. Chapman, The magnitude of corona point discharge current, J. Atmos. Sci. 34 (1977) 1801–1809.
[29] F.D. Alessandro, Experimental study of the effect of wind on positive and negative corona from a sharp point in a thunderstorm, J. Electrost. 67 (2009) 482–487.
[30] N.L. Aleksandrov, E.M. Bazelyan, R.B. Carpenter, M.M. Drabkin, Y.P. Raizer, The effect of coronae on leader initiation and development under thunderstorm conditions and in long air gaps, J. Phys. D. Appl. Phys. 34 (2001) 3256–3266.
[31] N.L. Aleksandrov, E.M. Bazelyan, Y.P. Raizer, Initiation and development of first lightning leader: the effects of coronae and position of lightning origin, Atmos. Res. 76 (2005) 307–329.
[32] N.L. Aleksandrov, E.M. Bazelyan, F.D. Alessandro, Y.P. Raizer, Dependence of

lightning rod efficacy on its geometric dimensions - a computer simulation, J. Phys. D. Appl. Phys. 38 (2005) 1225–1238.
[33] E.M. Bazelyan, Y.P. Raizer, N.L. Aleksandrov, Corona initiated from grounded objects under thunderstorm conditions and its influence on lightning attachment, Plasma Sources Sci. Technol. 17 (2008) 024015 (17pp).
[34] N.A. Kaptzov, Electricheskiye Yavleniya V Gazakh I Vacuume, OGIZ, Moscow, 1947.
[35] R. Morrow, The theory of positive glow corona, J. Phys. D. Appl. Phys. 30 (1997) 3099–3114.
[36] J.L. Davis, J.F. Hoburg, HVDC transmission line computations using finite elements and characteristics methods, J. Electrost. 18 (1986) 1–22.
[37] B.Y. Guo, J. Guo, A.B. Yu, Simulation of the electric field in wire-plate type electrostatic precipitators, J. Electrost. 72 (2014) 301–310.
[38] P. Atten, K. Adamiak, B. Khaddour, J.L. Coulomb, Simulation of corona discharge in configurations with a sharp electrode, J. Optoelectron. Adv. Mater. 6 (3) (2004) 1023–1028.
[39] P. Atten, J.-L. Coulomb, B. Khaddour, Modeling of electrical field modified by injected space charge, IEEE Trans. Magnetics 41 (2005) 1436–1439.
[40] A.J. Medlin, C.A.J. Fletcher, R. Morrow, A pseudotransient approach to steady state solution of electric field-space charge coupled problems, J. Electrost. 43 (1998) 39–60.
[41] J.S. Chang, D. Brocilo, K. Urashima, J. Dekowski, J. Podlinski, J. Mizeraczyk, G. Touchard, On-set of EHD turbulence for cylinder in cross flow under corona discharges, J. Electrost. 64 (2006) 569–573.
[42] A. Bayliss, M. Gunzburger, E. Turkel, Boundary conditions for the numerical solution of elliptic equations in exterior regions, SIAM J. Appl. Math. 42 (2) (1982) 430–451.
[43] N.C. Nguyen, J. Peraire, B. Cockburn, An implicit high-order hybridizable discontinuous Galerkin method for nonlinear convection diffusion equations, J. Comput. Phys. 228 (23) (2009) 8841–8855. http://linkinghub.elsevier.com/retrieve/pii/S0021999109004756.
[44] N.C. Nguyen, J. Peraire, B. Cockburn, An implicit high-order hybridizable discontinuous Galerkin method for the incompressible Navier-Stokes equations, J. Comput. Phys. 230 (4) (2011) 1147–1170. http://linkinghub.elsevier.com/retrieve/pii/S0021999110005887.
[45] N.C. Nguyen, J. Peraire, Hybridizable discontinuous Galerkin methods for partial differential equations in continuum mechanics, J. Comput. Phys. 231 (18) (2012) 5955–5988.
[46] G.W. Penney, R.E. Matick, Potentials in DC corona fields, Trans. Am. Inst. Electr. Eng. 79 (1960) 91–99.
[47] M. Hara, N. Hayashi, K. Shiotsuki, M. Akazaki, Influence of wind and conductor potential on distributions of electric field and ion current density and ground level in DC high voltage line to plane geometry, IEEE Trans. Power apparatus Syst. PAS 101 (4) (1982) 803–814.